Chemical Engineering Journal 214 (2013) 376–385

Contents lists available at SciVerse ScienceDirect

Chemical Engineering Journal

journal homepage: www.elsevier.com/locate/cej

Fabrication of β-cyclodextrin conjugated magnetic HNT/iron oxide composite for high-efficient decontamination of U(VI)

Shitong Yang [a,*], Pengfei Zong [b], Jun Hu [a], Guodong Sheng [c], Qi Wang [a], Xiangke Wang [a]

[a] Key Laboratory of Novel Thin Film Solar Cells, Institute of Plasma Physics, Chinese Academy of Sciences, P.O. Box 1126, 230031 Hefei, PR China
[b] School of Nuclear Science and Technology, Xi'an Jiaotong University, 710049 Xi'an, PR China
[c] School of Chemistry and Chemical Engineering, Shaoxing University, 312000 Shaoxing, PR China

HIGHLIGHTS

- A novel magnetic CD/HNT/iron oxide composite was synthesized by using chemical method.
- The maximum sorption amount of U(VI) on CD/HNT/iron oxide was higher than that on many other materials.
- CD/HNT/iron oxide exhibited satisfying removal efficacy for simulated mixed wastewater.
- CD/HNT/iron oxide could be easily separated from aqueous solution with a permanent magnet.
- CD/HNT/iron oxide could be used for the purification of actual U(VI)-bearing effluents.

ARTICLE INFO

Article history:
Received 31 July 2012
Received in revised form 19 October 2012
Accepted 22 October 2012
Available online 30 October 2012

Keywords:
CD/HNT/iron oxide composite
U(VI)
Sorption reversibility
Magnetic separation
Simulated effluent disposal

ABSTRACT

In this study, β-cyclodextrin (β-CD) was chemically grafted onto halloysite nanotube/iron oxides (HNT/iron oxides) to prepare a novel magnetic CD/HNT/iron oxide composite. The XRD pattern and FT-IR spectra analysis provide evidence for the successful grafting of β-CD on HNT/iron oxide surfaces. Elemental analysis indicates that the grafted β-CD amount in CD/HNT/iron oxide composite is 112 mg/g. Batch technique was adopted to investigate the removal efficiency of U(VI) from aqueous solutions by CD/HNT/iron oxide as a function of various environmental factors. The sorption reversibility and performance of CD/HNT/iron oxide in simulated effluent disposal were also tested. The sorption kinetic data can be well fitted by the pseudo-second-order model. The pH-dependent sorption suggests an optimal pH value of 7.0 for using CD/HNT/iron oxide in the decontamination of U(VI) from aqueous solutions. The sorption irreversibility at pH 5.5 was attributed to the inner-sphere binding of U(VI) on CD/HNT/iron oxide surface sites. The maximum sorption capacity of U(VI) on CD/HNT/iron oxide is considerably higher than that of some other reported materials. Related data show that CD/HNT/iron oxide exhibits satisfactory treatment efficiency for the simulated wastewater. It is worth noting that CD/HNT/iron oxide could be easily separated from aqueous solution by using a permanent magnet. By integrating the experimental results presented in this study, it is clear that CD/HNT/iron oxide can be potentially used as a cost-effective material for the purification of actual U(VI)-bearing effluents.

1. Introduction

Water radioactive pollution has become a serious environmental problem all over the world. A series of hazardous radionuclides (e.g., ^{235}U, ^{238}U, ^{235}Np, ^{239}Pu and ^{247}Cm, etc.) were discharged into aquatic systems through various nuclear processes, such as mining operations, refining of nuclear fuel, aboveground/underground nuclear tests, nuclear energy processing facilities and nuclear power plant accidents [1,2]. Uranium(VI), a chemical homolog of hexavalent actinides, is an irreplaceable material in nuclear fuel cycle. The potential risk of uranium-containing water system is a significant environmental concern due to its long half-life ($t_{1/2}$ (^{235}U) = $7.04 \times 10^8 a$; $t_{1/2}$ (^{238}U) = $4.47 \times 10^9 a$) [3]. Exposure to uranium can result in serious biochemical and radioactive harms to biological organization such as skin corrosion, toxic hepatitis, kidney damage, histopathological system damage and even cancers. In view of this point, a series of regulations have been proposed in the past decades to limit U(VI) concentration in environmental mediums. For instance, the guideline values for U(VI) concentration in drinking water were set to be 15 μg/L and 30 μg/L by World Health Organization and US Environmental Protection Agency, respectively [4].

* Corresponding author. Tel.: +86 551 5591368.
E-mail address: styang@ipp.ac.cn (S. Yang).

1385-8947/$ - see front matter © 2012 Elsevier B.V. All rights reserved.
http://dx.doi.org/10.1016/j.cej.2012.10.030

Besides, many European Union countries used *total indicative dose* (<0.1 mSv/y) as an additional guidance level for radionuclides in drinking water [5]. Hence, advanced techniques and materials are required to reduce U(VI) concentration in contaminated groundwater so as to meet the above-mentioned water quality standards.

Sorption technique is widely adopted in environmental protection field due to its convenient operation, low cost, high efficiency and environmental friendliness. Many kinds of materials such as clinoptilolite [6], activated carbon [7], coir pith [8] and trichoderma harzianum [9] are proved to be capable in the decontamination of U(VI)-bearing effluents. However, the difficulty in the separation and recovery of these materials from solution limits their further application. To compensate for this imperfection, the preparation of magnetic materials with high separation convenience has become a new research hotspot in recent years [10,11]. However, the introduced iron oxide on magnetic material surfaces brings adverse defects such as lower sorption capacity and poor dispersibility, which restrict their large-scale application in wastewater treatment and contaminated environment remediation. Fortunately, the two shortages mentioned above have been successfully remedied via the selective modification of magnetic materials with natural and synthetic polymers. As expected, the obtained composites exhibit excellent utility in the decontamination of heavy metal ions and organic pollutants [12,13].

Halloysite nanotubes (HNTs) are a kind of two-layered aluminosilicate clay with hollow nanotubular structure. Due to their novel physicochemical properties, HNTs have been widely used in various fields such as catalysis, electronics, biomedicine and functional materials [14,15]. Cyclodextrins (CDs), produced from the bacteria enzymatic degradation of starch, are torus-shaped cyclic oligosaccharide with an internal hydrophobic cavity. Specifically, β-cyclodextrin (β-CD) was proved to exhibit good performance in wastewater disposal. Herein, magnetic HNT/iron oxides were firstly synthesized by using co-precipitation method. Afterwards, β-CD was chemically grafted onto HNT/iron oxides to prepare a novel magnetic composite (denoted as CD/HNT/iron oxide). The obtained CD/HNT/iron oxide composite were characterized by transmission electron microscopy (TEM), X-ray powder diffraction (XRD), Fourier transform infrared (FT-IR) spectroscopy and zeta potential analysis. In addition, elemental analysis was conducted to quantitatively determine the grafted amount of β-CD in CD/HNT/iron oxide composite. Batch technique was adopted to investigate the sorption performances of CD/HNT/iron oxide composite towards U(VI) as affected by various environmental conditions. Further experiment was conducted to test its application potential in simulated wastewater disposal.

2. Experimental details

2.1. Materials and reagents

The sample of HNTs was obtained from Shinshi metallurgy chemical Co., Ltd., (Guangzhou, China) as a gift. The HNT powder was rinsed with Milli-Q water and then dried at 80 °C in an oven. The derived sample was milled and passed through a 200-mesh screen to gain small-sized solid particles with larger surface area and better dispersion. The specific surface area of bare HNTs was measured to be 48.2 m^2/g by using N_2-BET method. All the other chemicals were purchased from Sinopharm Chemical Reagent Co., Ltd., (Shanghai, China) in analytical purity and used directly without any further purification. All the reagents were prepared with Milli-Q water.

2.2. Preparation of β-CD conjugated HNT/iron oxides

The HNT/iron oxide composite was prepared under N_2 condition via two sequential processes, i.e., a wet impregnation process followed by a co-precipitation process. In brief, 1.5 g HNTs was added into a 200 mL solution containing 2.98 g $FeCl_3{\cdot}6H_2O$ and 1.53 g $FeSO_4{\cdot}7H_2O$. During the initial wet impregnation process with continuous magnetic agitating, the positive Fe^{2+} and Fe^{3+} ions were introduced on HNT surfaces through complexation reactions. Afterwards, ~40 mL NaOH solution (0.5 mol/L) was dripped into the mixture to precipitate the surface-immobilized Fe^{2+} and Fe^{3+} ions. The mixture pH was maintained at ~11 to ensure the complete transformation of iron ions to iron oxides. The reaction was conducted at 70 °C for 3 h under constant magnetic stirring. The as-prepared HNT/iron oxide composite was repeatedly washed with Milli-Q water and dried at 105 °C for 4 h. The CD/HNT/iron oxide composite was prepared via the following procedures: Firstly, 1.0 g HNT/iron oxides was added to 20 mL phosphate buffer (0.005 mol/L, pH 6.5) and sonicated for 15 min. Afterwards, 5.0 mL carbodiimide solution was added and the mixture was further sonicated for 30 min. Finally, 0.3 g β-CD was added and the formed mixture was continuously sonicated for 120 min. This addition dosage is obtained from the effect of added β-CD content in solution on the grafted β-CD amount on HNT/iron oxides (see Supplementary Material Fig. S1). The as-prepared magnetic CD/HNT/iron oxide composite was recovered from the mixture with a permanent magnet and then dried in a vacuum oven.

2.3. Characterization

The microscopic morphology of bare HNTs and CD/HNT/iron oxide composite were characterized by transmission electron microscopy (TEM). Drops of bare HNT (or CD/HNT/iron oxide) aqueous suspensions were delivered onto the copper grid and dried in air. Afterwards, the TEM images were collected by using JEOL-2010 microscope. The XRD patterns of bare HNTs, HNT/iron oxides and CD/HNT/iron oxide were recorded on a MAC Science Co., M18XHF diffractometer using Cu Kα radiation. The measurements were carried out in the 2θ range of 10°–70° with a scanning step-length of 0.02°. The FTIR spectra of bare HNTs, HNT/iron oxides, CD/HNT/iron oxide and pure β-CD were recorded with a FTIR spectrometer (Perkin–Elmer spectrum 100, America) in the range of 4000–400 cm^{-1} by using KBr pellets. The spectral resolution was set to 1 cm^{-1} and 150 scans were collected for each spectrum. The magnetic measurements were performed in a MPMS-XL SQUID magnetometer. For zeta potential measurements, a series of CD/HNT/iron oxide suspensions (0.5 g/L) were prepared in 0.01 mol/L $NaNO_3$ solution. The gained suspensions were adjusted to different pH values with tiny amount of 0.01 mol/L HNO_3/NaOH solutions and sonicated for 10 min in an ultrasonic bath. The zeta potential of each suspension was measured by using Zetasizer Nano ZS Analyzer. The zero point charge (pH_{zpc}) was obtained by interpolating the data to zero zeta potential.

2.4. Dispersion in aqueous solution

To establish the correlation between solid concentration and the dispersion in aqueous solution, the UV–vis spectra of bare HNTs and CD/HNT/iron oxide with different concentrations were scanned by using SHIMADZU UV–vis 2550 spectrophotometer in the wavelength range of 190–800 nm.

2.5. Experimental procedure

All the experiments were conducted in polyethylene centrifuge tubes by using batch technique. Briefly, the suspensions of CD/HNT/iron oxide and background electrolyte solution were pre-equilibrated for 24 h, and then U(VI) stock solution and complexing ligands were seriatim added to achieve the desired concentrations of individual components. The pH was adjusted to desired values

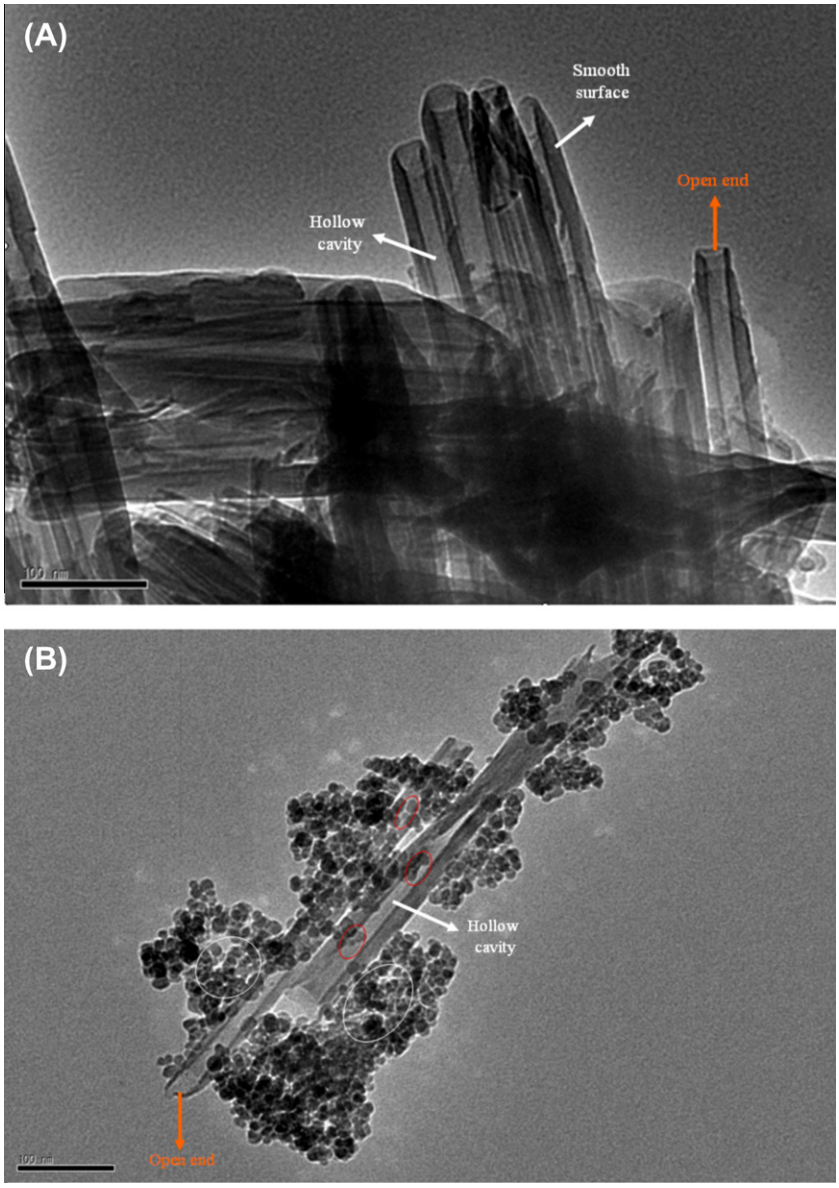

Fig. 1. TEM images of bare HNTs (A) and CD/HNT/iron oxide composite (B).

by adding negligible volumes of 0.1 or 0.01 mol/L HNO_3 or NaOH solutions. The centrifuge tubes were gently shaken on a rotating oscillator for 24 h to achieve sorption equilibrium. Afterwards, the samples were exposed to a permanent magnet to separate solid and liquid phases. The concentrations of U(VI) in the supernatant were measured by using U Arsenazo-III spectrophotometry at 650 nm. The sorption percent (sorption% = $(C_0 - C_e)/C_0 \times 100\%$) and sorption amount ($q_e = (C_0 - C_e)\cdot V/m$) were then calculated from the initial U(VI) concentration (C_0), the final U(VI) concentration (C_e), the CD/HNT/iron oxide mass (m) and the suspension volume (V).

3. Results and discussion

3.1. Characterization

Fig. 1A and B shows the TEM images of bare HNTs and CD/HNT/iron oxide, respectively. As can be seen from Fig. 1A, bare HNTs exhibit straight tubular morphology with smooth external surface, open ends and hollow cavity of ~20 nm in diameter. It is clear from Fig. 1B that the HNT surfaces are coated with iron oxide clusters (marked with white cycles), which are composed of smaller subunits of ~10 nm in diameter. Besides, some iron oxide particles are found to adhere on the inner wall of HNT hollow cavities (marked with red[1] circles). No detectable layer due to grafted β-CD can be observed from the TEM image, which may be attributed to the overlap of β-CD by the surface-coated iron oxide particles. Herein, it is worth noting that the HNT substrate in CD/HNT/iron oxide still possesses open-ended structure. The open ends, hydroxyl-containing surface and hollow cavities are conductive to the attachment of heavy metal ions and radionuclides onto CD/HNT/iron oxide.

Fig. 2 shows the XRD patterns of bare HNTs, HNT/iron oxides and CD/HNT/iron oxide composite. For bare HNTs, the diffraction peaks at 12.1°, 20.1°, 24.3°, 35.4°, 38.9°, 55.2° and 63.3° are corresponded to the characteristic (001), (100), (002), (110), (003), (210) and (300) planes of halloysite-7 Å with hexagonal structure

[1] For interpretation of color in Fig. 1, the reader is referred to the web version of this article.

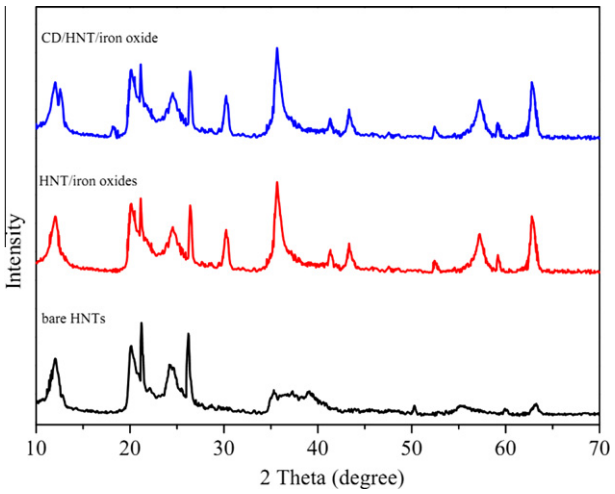

Fig. 2. XRD patterns of bare HNTs, HNT/iron oxides and CD/HNT/iron oxide composite.

(JCPDS Card No. 29-1487). The diffraction angle of (001) plane (herein, 12.1°) corresponds to the characteristic basal spacing of halloysite-7 Å mineral (i.e., 0.72 nm). Furthermore, the broad diffraction peaks manifest that the bare HNTs are in small crystal size and poor crystallinity degree. Compared with bare HNTs, the XRD pattern of HNT/iron oxides displays five new peaks at 30.1°, 35.6°, 43.3°, 57.1° and 62.7°, which can be assigned to the characteristic peaks of cubic magnetite phase (JCPD No. 89-3854). The other two peaks at 41.3° and 59.2° may correspond to goethite phase formed on HNT surfaces. In the XRD pattern of CD/MWCNT/iron oxide composite, the appearance of two sharp peaks at 12.7° and 18.3° manifests the introduction of β-CD on HNT/iron oxide surfaces [16].

Fig. 3 illustrates the FTIR spectra of bare HNTs (curve A), HNT/iron oxides (curve B), CD/HNT/iron oxide (curve C) and pure β-CD (curve D). For bare HNTs (curve A), the double bands at 3699 and 3622 cm^{-1} correspond to O–H stretching vibrations of inner-surface hydroxyl groups and inner hydroxyl groups, respectively [17]. The bands at 3453 and 1640 cm^{-1} are assigned to O–H stretching vibration of adsorbed water. The bands at 1097 and 1035 cm^{-1} are attributed to apical Si–O and Si–O–Si stretching vibrations, respectively. The band at 912 cm^{-1} arises from O–H

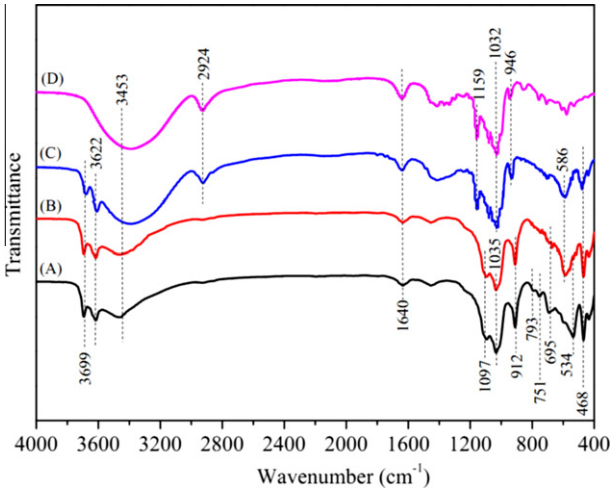

Fig. 3. FTIR spectra of bare HNTs (curve A), HNT/iron oxides (curve B), CD/HNT/iron oxide composite (curve C) and pure β-CD (curve D).

deformation vibration of inner Al–O–H groups. The band at 793 cm^{-1} is assigned to Si–O symmetric stretching vibration. The bands at 751 and 695 cm^{-1} derive from perpendicular Si–O stretching vibration. The bands at 534 and 468 cm^{-1} are attributed to Si–O–Si and Al–O–Si deformation vibrations, respectively. The FTIR spectrum of HNT/iron oxides (curve B) includes all the above-mentioned peaks in bare HNTs (curve A). Specifically, the slight broadened band at 3453 cm^{-1} is attributed to the stretching vibrations of hydroxyl groups from iron oxides [18]. In addition, the peak at 586 cm^{-1} is corresponded to the characteristic Fe–O stretching vibration of iron oxides. In the spectrum of pure β-CD (curve D), the broad band at 3300–3500 cm^{-1} is attributed to –OH stretching vibration. The band at 2924 cm^{-1} corresponds to asymmetric C–H stretching vibration [19]. The bands at 1159 and 1032 cm^{-1} derive from the coupled C–C/C–O stretch vibration and antisymmetric glycosidic C–O–C vibration, respectively [20]. The band at 946 cm^{-1} is assigned to the R-1, 4-bond skeleton vibration. All these characteristic bands are present in the spectrum of CD/HNT/iron oxide (curve C), which provides direct evidence for the successful grafting of β-CD on HNT/iron oxide surfaces. Elemental analysis suggests that the grafted β-CD amount in CD/HNT/iron oxide is 112 mg/g (i.e., 11.2% in w/w). The magnetization curves have been previously used to quantitatively determine the grafted amount of natural organic matter on solid particles [21]. Herein, the saturation magnetization of HNT/iron oxides and CD/HNT/iron oxide are measured to be 28.54 and 25.26 emu/g, respectively. The difference of 3.28 emu/g suggests that the β-CD content in CD/HNT/iron oxide is 11.5% (w/w), which is accordance with that calculated from elemental analysis (11.2% in w/w). Meanwhile, the good magnetic property makes it easy to separate CD/HNT/iron oxide from aqueous solutions with an external magnet.

Fig. S2 illustrates the zeta potential of CD/HNT/iron oxide composite in 0.01 mol/L $NaNO_3$ solution as a function of pH values. It is clear that the zeta potential decreases from 18 eV to zero as pH increases from 2.0 to 4.8, then decreases rapidly to −39 mV as pH values rises up to 10.0. Thereby, the pH_{zpc} of CD/HNT/iron oxide composite is identified to be ~4.8. This variation trend in surface charge with greatly influence the sorption affinity of CD/HNT/iron oxide towards U(VI) at various pH values.

3.2. Dispersion in aqueous solution

Fig. 4 illustrates the UV–vis spectra of bare HNTs and CD/HNT/iron oxide in aqueous solution at various concentrations (0.4–4.2 g/L). The absorption peak at 210 nm can be assigned to the characteristic absorption of HNTs. As shown in Fig. 4A, the absorbance of bare HNT suspension at 210 nm increases from 0.38 to 4.67 as the relative concentration increases from 0.4 to 4.2 g/L. However, the absorbance reaches the maximum detection value of 5.00 as the relative concentration increases to 5.0 g/L. This phenomenon can be attributed to the complete absorption of UV light by the deep-colored HNT suspension. Similarly, the absorbance of CD/HNT/iron oxide suspension at 210 nm increases from 0.96 to 4.93 as the relative concentration increases from 0.4 to 3.6 g/L, and then reaches the maximum absorbance as the relative concentration increases to 4.2 g/L (Fig. 4B). Compared with bare HNT suspension, the CD/HNT/iron oxide suspension reaches the maximum absorbance at lower concentration due to its deeper color. The straight lines inserted in Fig. 4A and B describe the relevance between the absorbance and relative bare HNT (or CD/HNT/iron oxide) concentrations. The correlation coefficient of CD/HNT/iron oxide (R^2 = 0.9991) is higher than that of bare HNTs (R^2 = 0.9705). It is clear that CD/HNT/iron oxide suspension well follows the Lambert–Beer's law, which suggests that CD/HNT/iron oxide exhibits good dispersion in aqueous solution. Besides,

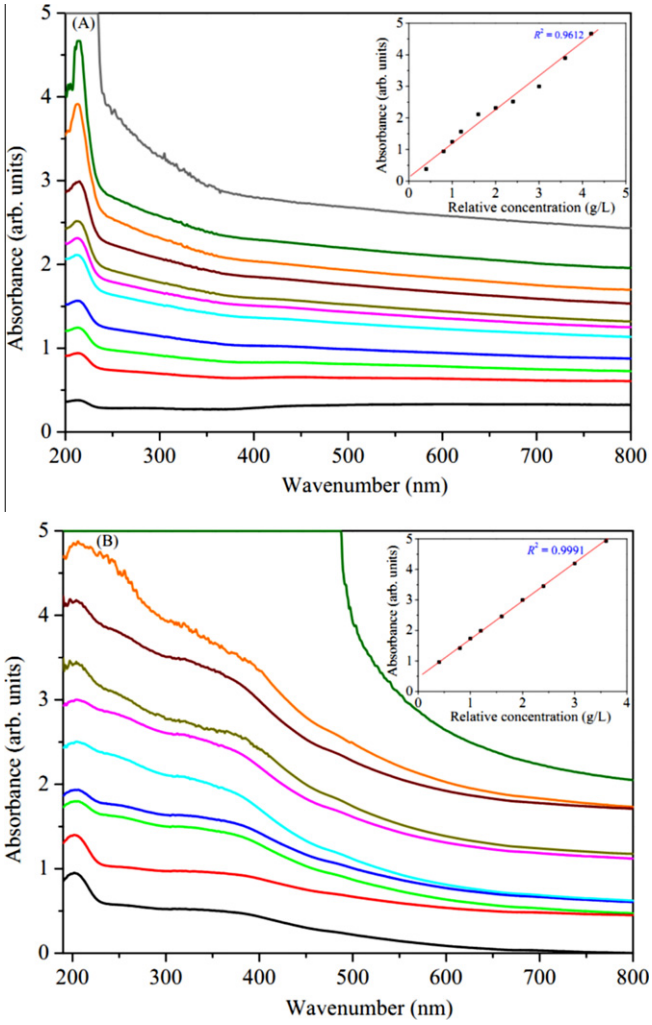

Fig. 4. UV–vis absorption spectra of bare HNTs (A) and CD/HNT/iron oxide composite (B) in aqueous solutions. Inset: Lambert–Beer's plots for the absorption peak of bare HNTs (A) and CD/HNT/iron oxide composite (B) at 210 nm.

sonication of CD/HNT/iron oxide suspension exhibits no influence on the absorption peak intensity. This phenomenon manifests that β-CD has been grafted on HNT/iron oxide surfaces via chemical interaction rather than physical sorption [13,22].

3.3. Effect of contact time

Fig. 5 shows the capture of U(VI) by CD/HNT/iron oxide as a function of contact time and initial U(VI) concentration. It is clear that the sorption amount of U(VI) increases with increasing contact time and initial U(VI) concentration. The sorption of U(VI) increases fast in the first 1 h, and then slowed down until the sorption process achieves equilibrium after 4 h. Herein, it is worth noting that the instantaneous time for separating CD/HNT/iron oxide composite from solution by external magnet can be neglected when testing the total contact time. The fast removal rate during the initial stage may be attributed to the rapid diffusion of U(VI) from the solution to the external surfaces of CD/HNT/iron oxide. As the sites being gradually occupied, the adsorbed U(VI) tends to be transported from the bulk phase to the actual sorption sites (i.e., inner-sphere pores of CD/HNT/iron oxide) [23]. Such slow diffusion process will decrease the sorption rate of U(VI) at later stages. Overall, the removal process is quite fast and 4 h is enough to reach equilibrium, indicating that CD/HNT/iron oxide

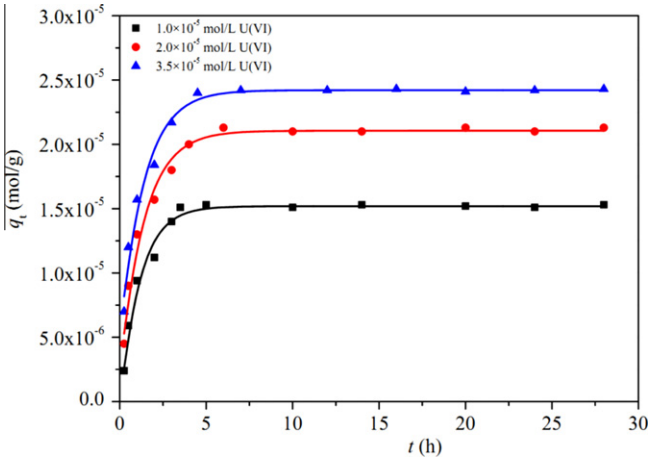

Fig. 5. Sorption of U(VI) on CD/HNT/iron oxide composite as a function of contact time and initial U(VI) concentrations. T = 298 K, pH = 5.5, m/V = 0.5 g/L, I = 0.01 mol/L $NaNO_3$.

can be potentially applied in continuous effluent disposal. The equilibrium sorption amount increases from 1.52×10^{-5} to 2.42×10^{-5} mol/g as the initial U(VI) concentration increases from 1.0×10^{-5} to 3.5×10^{-5} mol/L. This upward trend is reasonable due to the fact that the greater concentration gradient at higher initial U(VI) concentration can provide stronger driving force for U(VI) uptake [24]. According to the above results, the shaking time is fixed at 48 h in the following experiments to ensure that the removal process can achieve complete equilibrium.

The surface characteristics and diffusion resistance of solid particles play an important role in sorption rate and accordingly the overall solute migration. Therefore, the application of appropriate kinetic models can provide useful information for determining the underlying mechanisms during the entire sorption process. In view of this point, the experimental kinetic data are simulated by the pseudo-first-order ($\ln(q_e - q_t) = \ln q_e - k_1 t$) and pseudo-second-order ($\frac{t}{q_t} = \frac{1}{k_2 q_e^2} + \frac{1}{q_e} t$) models [25,26]. Herein, q_e and q_t refer to the sorption capacity of U(VI) (mol/g) at equilibrium time and time t (h), respectively; k_1 (h^{-1}) and k_2 (g/(mol h)) are the rate constants of pseudo-first-order and pseudo-second-order equation, respectively. The slope and intercept of the linear plot of $\ln(q_e - q_t)$ versus t are used to calculate k_1 and $q_{e,cal}$, respectively. The slope and intercept of the plot of t/q_t versus t are used to determine $q_{e,cal}$ and k_2, respectively. The obtained kinetic parameters from both model fits are listed in Table 1. The correlation coefficients (R^2) for pseudo-second-order model are higher than those for pseudo-first-order model. In addition, the q_e values ($q_{e,cal}$) obtained from pseudo-second-order model fitting are more close to the experimental q_e values ($q_{e,exp}$). The fact that the kinetic data are accordance with pseudo-second-order model suggests chemisorption may be the rate-controlling mechanism rather than physical sorption [27].

3.4. Effect of pH and ionic strength

Solution pH has a significant influence on the migration and transformation behaviors of environmental contaminants at solid/water interfaces. In view of this point, the pH-dependent sorption of U(VI) on CD/HNT/iron oxide composite was investigated at various electrolyte concentrations, i.e., 0.001, 0.005, 0.01, 0.05 and 0.1 mol/L $NaNO_3$ solutions, respectively. As shown in Fig. 6, the sorption percentage of U(VI) in 0.01 mol/L $NaNO_3$ solution increases gradually from ~10% to 40% as pH increases from 2.0 to 5.0 (Region I), and then sharply increases to ~92% as pH reaches

Table 1
The kinetic parameters of U(VI) sorption on CD/HNT/iron oxide.

Correlation parameters		Initial U(VI) concentration (mol/L)		
		1.0×10^{-5}	2.0×10^{-5}	3.5×10^{-5}
Pseudo-first-order	k_1 (h^{-1})	1.230	0.958	0.640
	$q_{e,exp}$ (mol/g)	1.52×10^{-5}	2.12×10^{-5}	2.42×10^{-5}
	$q_{e,cal}$ (mol/g)	1.24×10^{-5}	1.75×10^{-5}	2.01×10^{-5}
	R^2	0.920	0.982	0.965
Pseudo-second-order	k_2 (g/(mol h))	1.31×10^{5}	9.81×10^{4}	6.24×10^{4}
	$q_{e,exp}$ (mol/g)	1.52×10^{-5}	2.12×10^{-5}	2.42×10^{-5}
	$q_{e,cal}$ (mol/g)	1.56×10^{-5}	2.18×10^{-5}	2.47×10^{-5}
	R^2	0.999	0.999	0.999

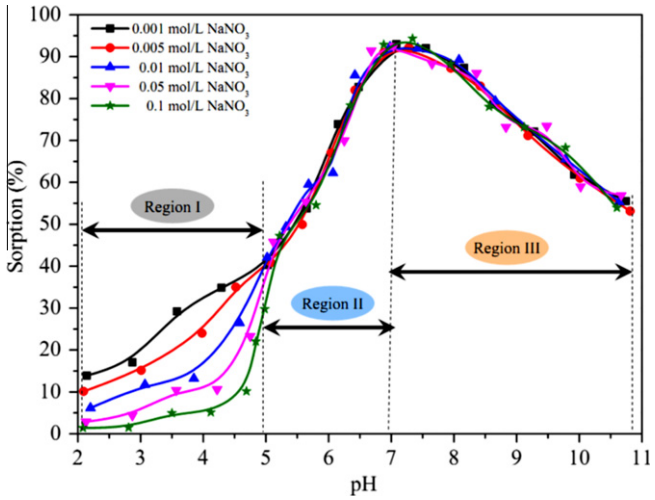

Fig. 6. Effect of ionic strength on U(VI) sorption as a function of pH values. T = 298 K, m/V = 0.5 g/L, $C_{(U(VI))initial}$ = 2.0×10^{-5} mol/L.

to 7.0 (region II). Afterwards, the sorption percentage sharply decreases from ~92% to ~52% in the pH range of 7.0–11.0 (region III). The presence of three sorption regions manifests the occurrence of multifarious sequestration approaches [28].

The observed sorption trends are related with the surface properties of CD/HNT/iron oxide and the distribution of U(VI) species in solution. As mentioned above, the CD/HNT/iron oxide surfaces are positively charged at pH < pH_{zpc} (i.e., ~4.8). Fig. S3 illustrates the relative proportion of U(VI) species computed by Visual MINTEQ ver. 2.61 [29]. At pH < 5.0, the predominant U(VI) species is UO_2^{2+}, which is difficult to be captured by positively-charged CD/HNT/iron oxide due to electrostatic repulsion. As shown in Fig. S2, the surface of CD/HNT/iron oxide becomes negatively charged at pH > 4.8 and the surface electronegativity enhances with increasing pH values. Besides, the surface sites become more dissociated at higher pH values. These two variation trends enhance the complexation ability of CD/HNT/iron oxide towards hydrolyzed U(VI)-OH^- species (e.g., $(UO_2)_3(OH)_5^+$ and $(UO_2)_4(OH)_7^+$) in the pH range of 5.0–7.0. As shown in Fig. S3, the relative proportions of $(UO_2)_3(OH)_5^+$ and $(UO_2)_4(OH)_7^+$ decrease at pH > 7.0 and U(VI) species are mainly present as negatively-charged $UO_2(OH)_3^-$ and $(UO_2)_3(OH)_7^-$. These two species are difficult to be immobilized on the negatively-charged surfaces of CD/HNT/iron oxide due to electrostatic repulsion, which results in the decreases of U(VI) immobilization in this pH range. Based on the pH-dependent sorption curve, an optimal pH value of 7.0 should be selected when using CD/HNT/iron oxide for the purification of U(VI)-containing wastewater.

Evaluation of ionic strength effect on sequestration behavior is helpful to verify the application potential of solid materials in sewage purification. As shown in Fig. 6, the removal of U(VI) is strongly influenced by ionic strength variation at pH < 5.0, suggesting that electrostatic interaction or outer-sphere complexation is the dominant mechanism in this pH range [30,31]. Specifically, the removal percentage of U(VI) decreases with increasing $NaNO_3$ solution concentration. The activity of U(VI) ions in solution is greatly reduced at higher ionic strength, which accordingly limits their migration to CD/HNT/iron oxide surfaces. Besides, higher ionic strength will reduce the electrostatic repulsion between CD/HNT/iron oxide particles, which causes their aggregation and decreases the uptake of U(VI). The ionic strength-independence of U(VI) uptake at pH > 5.0 is indicative of an inner-sphere complexation mechanism.

3.5. Effect of solid content

Fig. 7 shows the sorption of U(VI) on iron oxides, bare HNTs, HNT/iron oxides and CD/HNT/iron oxide at various solid content. Despite the specific surface area of CD/HNT/iron oxide (34.3 m^2/g) is lower than that of HNT/iron oxides (38.6 m^2/g) and bare HNTs (48.2 m^2/g), the sorption percentage of U(VI) on CD/HNT/iron oxide composite is higher than that on HNT/iron oxides and bare HNTs (Fig. 7A). This inconsistency manifests that the specific surface area is not the decisive factor for U(VI) sorption. Alternatively, the grafted β-CD is expected to enhance the sorption capacity of CD/HNT/iron oxide composite. The truncated-cone structure of β-CD contains an apolar cylindrical cavity with primary hydroxyl sites lying on the external surface and secondary hydroxyl sites lying on the internal surface [32]. It is clear that CD/HNT/iron oxide surfaces comprise two kinds of functional groups, i.e., the hydroxyl sites that originally exist on HNT/iron oxide surfaces together with those introduced by the grafted β-CD. The strong complexation capacity of these hydroxyl sites towards U(VI) contribute to the enhanced removal capacity of CD/MWCNT/iron oxide composite. In addition, the grafted β-CD greatly enhances the dispersion of CD/HNT/iron oxide composite (UV–vis spectra in Fig. 4B), which improves the availability of surface hydroxyl sites for binding U(VI). This is another tentative interpretation for the higher removal capacity of CD/HNT/iron oxide composite.

As can be seen from Fig. 7A, the sorption percentage of U(VI) increases from ~30% to ~72% as the CD/HNT/iron oxide content (m/V) increases from 0.1 to 1.0 g/L, and then its increase is negligible at m/V > 1.0 g/L. The number of functional groups at CD/HNT/iron oxide surfaces increases with increasing solid contents. As a result, more binding sites are available to form complexes with U(VI). From the aspect of reducing sewage treatment cost, the optimal content for CD/HNT/iron oxide to decontaminate U(VI) at pH 5.5 is 1.0 g/L. One can see from Fig. 7B that the sorption amount of U(VI) decreases gradually with increasing CD/HNT/iron oxide content. The interactions between solid particles may desorb some weak-linked U(VI) ions from CD/HNT/iron oxide surfaces. In addition, higher solid content may increase the aggregation probability of CD/HNT/iron oxide particles and thereby decrease the total surface area, which leads to the decrease of U(VI) sorption amount.

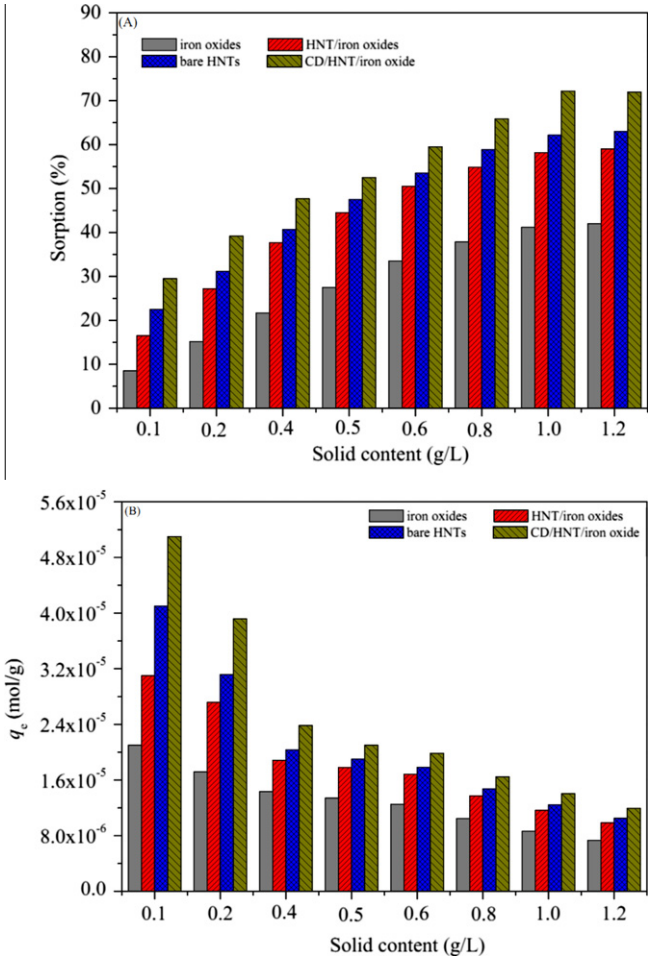

Fig. 7. Sorption percentage (A) and sorption amount (B) of U(VI) on iron oxides, bare HNTs, HNT/iron oxides and CD/HNT/iron oxide composite as a function of solid content. T = 298 K, pH = 5.5, $C_{(U(VI))initial}$ = 2.0 × 10^{-5} mol/L, I = 0.01 mol/L $NaNO_3$.

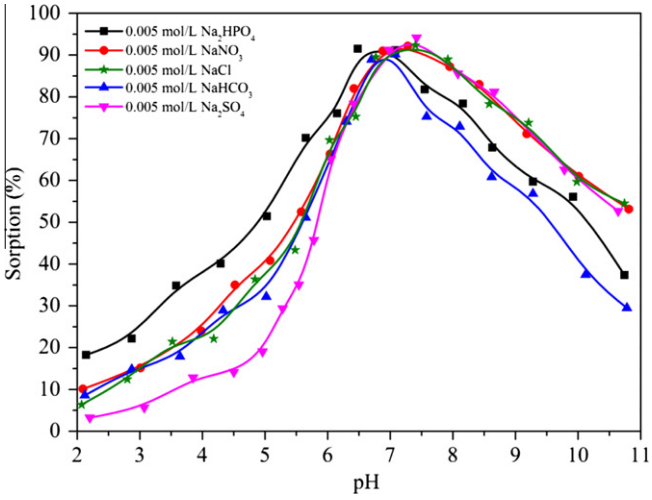

Fig. 8. Influence of coexisted ligands on the sorption of U(VI) on CD/HNT/iron oxide composite. T = 298 K, m/V = 0.5 g/L, $C_{(U(VI))initial}$ = 2.0 × 10^{-5} mol/L.

The introduction of iron oxide on HNT surfaces plays an important role in improving the separation performance of HNTs. As shown in Fig. 7A and B, the sorption percentage and sorption amount of U(VI) on bare HNTs are slightly higher than those on HNT/iron oxides. However, one should keep in mind that it is discommodious to separate bare HNTs from aqueous solution. The two commonly used methods, i.e., centrifugation and filtration are unsatisfactory due to the fact that high speed centrifugation consumes vast electric energy and filtration is prone to filter blockages. This imperfection significantly limits their further application in wastewater treatment and contaminated environment remediation. Although the introduction of iron oxide slightly decreases the sorption performance of HNT/iron oxides towards U(VI), the magnetic HNT/iron oxides can be easily separated from aqueous solution by using an external magnet. The high separation convenience is expected to reduce the cost of using HNT/iron oxides in wastewater disposal. Besides, the slightly decreased sorption performance of HNT/iron oxides can be compensated by the grafted β-CD. As shown in Fig. 7A and B, the prepared CD/HNT/iron oxide exhibits favorable sorption percentage and sorption amount towards U(VI). Meanwhile, the high separation convenience of magnetic CD/HNT/iron oxide further ensures its actual applicability in wastewater purification.

3.6. Effect of coexisted ligands

Multiple components are simultaneously present in natural water and wastewater systems. Inorganic anions, with high chemical reactivity and strong complexation ability towards both metal ions and solid surfaces, can significantly affect the mobility and bioavailability of pollutants in environmental mediums. In view of this point, it is crucial to investigate the effect of coexisted ligands on the decontamination of U(VI)-polluted water systems.

Fig. 8 shows the effect of coexisted ligands on U(VI) immobilization as a function of pH values. To help discriminate and analyze the role of various inorganic anions, related experiments were processed in NaX (X represents electrolyte anions) solutions. As shown in Fig. 8, the sequestration of U(VI) on CD/HNT/iron oxide is greatly influenced by inorganic anion ligands. Taking the sequestration of U(VI) in NO_3^- electrolyte solution as a point of reference, one can see that Cl^- has no obvious effect on U(VI) sorption over the whole pH range. The presence of CO_3^{2-} has no distinct influence on U(VI) sorption at pH < 7.0, while significantly reduces U(VI) sorption at higher pH values. The presence of SO_4^{2-} greatly reduces U(VI) immobilization at pH < 6.0, while no distinct influence is observed at higher pH values. In contrast, the effect of PO_4^{3-} can be divided into two parts, i.e., enhancing U(VI) sequestration at pH < 7.0, while reducing U(VI) sequestration at pH > 7.0.

Briefly, electrolyte anions may influence metal ion sequestration via site competition, alteration of surface charge, and the formation of solution complexes, ternary complexes and/or surface precipitates [33,34]. Herein, the distinct effects of different inorganic ligands on U(VI) immobilization may be attributed to their complexation with U(VI) species. Specifically, the inconspicuous effect of Cl^- is attributed to the similarity between U(VI) species in 0.005 mol/L NaCl solution and that in 0.005 mol/L $NaNO_3$ solution (figure not shown). The similarity between the U(VI) immobilization in CO_3^{2-}-containing system and in CO_3^{2-}-free system at pH < 7.0 is expected due to the presence of same U(VI) species such as UO_2^{2+}, UO_2OH^+ and $(UO_2)_3(OH)_5^+$) (Fig. S4A). The sharp decrease of U(VI) immobilization at pH > 7.0 may arise from the formation of strong $U(VI)-CO_3^{2-}$ complexes (e.g., $UO_2(CO_3)_3^{4-}$ and $UO_2(CO_3)_2^{2-}$) in solution (Fig. S4A). These results are in accordance with the sorption of U(VI) on goethite and hematite [35,36]. The negative effect of SO_4^{2-} at pH < 6.0 is a complex situation and needs an in-depth discussion. From the aspect of electrostatic interaction, the formation of negatively-charged $U(VI)-SO_4^{2-}$ complex (e.g., $UO_2(SO_4)_2^{2-}$ in Fig. S4B) would decrease the electropositivity of U(VI) ions and reduce the electrostatic barrier that U(VI) must overcome when immobilized on the positively-charged CD/HNT/

iron oxide surfaces. This would increase the immobilization of U(VI) on CD/HNT/iron oxide to some extent. It is reported that SO_4^{2-} could be adsorbed on solid surfaces via outer-sphere/inner-sphere complexation [37,38]. The adsorbed SO_4^{2-} would increase the surface electronegativity of CD/HNT/iron oxide and create a favorable electrostatic environment for U(VI) sequestration. Herein, the experimental phenomenon manifests that the competition of SO_4^{2-} with U(VI) for CD/HNT/iron oxide surface sites is expected to be the most reasonable explanation for the reduction of U(VI) sequestration in SO_4^{2-} containing system. At pH > 6.0, the U(VI) species are dominated by hydrolyzed U(VI)-OH^- complexes instead of U(VI) – SO_4^{2-} complexes (Fig. S4B), which leads to the similar U(VI) sorption trend in SO_4^{2-}-containing system to that in SO_4^{2-}-free system.

In contrast, the effect of PO_4^{3-} on U(VI) immobilization are distinct in two sequential pH ranges, which requires an in-depth discussion to infer the intrinsic mechanisms. Specifically, the positive action of PO_4^{3-} at pH < 7.0 may arise from the formation of surface precipitates and/or ternary surface complexes. To verify the specific binding mode, blank experiment was conducted in the system containing U(VI) and PO_4^{3-} but no CD/HNT/iron oxide at various pH values. The analysis results show no decrease in U(VI) equilibrium concentration in the whole pH range, which rules out the formation of surface precipitates. Hence, one can conclude that the enhancement of U(VI) immobilization in PO_4^{3-}-containing system is attributed to the formation of ternary surface complexes. Previous literature reported that U(VI) was strongly immobilized on heterogeneous subsurface media in the form of inner-sphere U(VI) – PO_4^{3-} complexes [39]. With the aid of surface complexation model (SCM) simulation, Cheng et al. ascribed the increased U(VI) uptake onto goethite-coated sand in PO_4^{3-}-containing system to the formation of "ligand-bridging" S-PO_4-UO_2 ternary complexes (S represents the surfaces sites) [40]. Similar structure was observed for hydroxyapatite-U(VI) – PO_4^{3-} system by X-ray absorption spectroscopic analysis [41]. The formation of ternary surface complexes will simultaneously decrease the mobility of U(VI) and PO_4^{3-} in aquatic systems and therefore reduce their potential ecological hazards. Hence, the stoichiometry, microstructure and thermodynamic stability of the proposed ternary complex herein need to be confirmed so as to further evaluate the performance of CD/HNT/iron oxide composite in U(VI)- and PO_4^{3-}-bearing effluent. As shown in Fig. S4C, the U(VI) species in the presence of 0.005 mol/L PO_4^{3-} are mainly present as negatively-charged $UO_2PO_4^-$ and $UO_2(OH)_3^-$ at pH > 7.0. These two species are difficult to be immobilized on the negatively-charged surfaces of CD/HNT/iron oxide due to electrostatic repulsion, which results in the decreases of U(VI) immobilization in this pH range.

3.7. Sorption and desorption isotherms

To further verify the binding mode and corresponding sorption reversibility of U(VI) on CD/HNT/iron oxide composite, the sorption and desorption experiments were carried out at two different pH values, i.e., pH 4.0 and pH 5.5. Specifically, the desorption isotherm at pH 4.0 overlaps well with the sorption isotherm (Fig. 9), which indicates that the sorption process under this condition is nearly reversible. This phenomenon manifests that the capture of U(VI) is mainly dominated by ion exchange with H^+/Na^+ at CD/HNT/iron oxide surfaces, forming an outer-sphere complex [42]. This kind of U(VI) species still maintains its hydrated sheath, which makes it easy to be influenced by environmental conditions due to the absence of a surface bond. Hence, one can consider the recovery of U(VI) and regeneration of CD/HNT/iron oxide by rinsing the U(VI)-immobilized CD/HNT/iron oxide with acidic water. In contrast, an obvious hysteresis is observed in the forward-sorption and backward-desorption process at pH 5.5, which may be attributed to the inner-sphere binding of U(VI) on CD/HNT/iron oxide surface sites [43]. Obviously, the formed complex is considered to be thermodynamic stable due to the formation of a tight bond. In view of this point, CD/HNT/iron oxide composite can be used as an effective backfill material for high level radioactive waste repository.

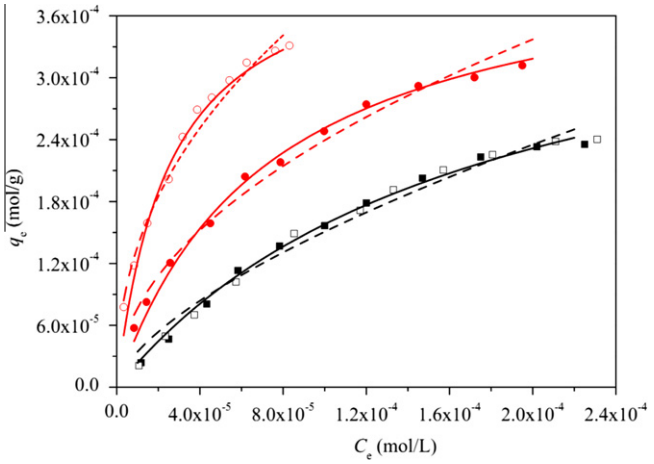

Fig. 9. Sorption–desorption isotherms and related model fittings of U(VI) on CD/HNT/iron oxide composite at pH 4.0 and 5.5. T = 298 K, m/V = 0.5 g/L, I = 0.01 mol/L $NaNO_3$. Symbols (■) and (□) denote the sorption and desorption data at pH 4.0, symbols (○) and (●) denote the sorption and desorption data at pH 5.5, solid lines represent the model fitting of Langmuir equation and dash lines represent the model fitting of Freundlich equation.

The sorption and desorption isotherms are simulated by Langmuir ($q_e = \frac{bq_{max}Ce}{1+bCe}$) and Freundlich ($q_e = K_F C_e^n$) equations (see Fig. 9). Herein, C_e is the equilibrium concentration of U(VI) remained in the solution (mol/L); q_e is the amount of U(VI) adsorbed on per weight unit of CD/HNT/iron oxide after equilibrium (mol/g); q_{max}, the maximum sorption capacity, is the amount of U(VI) at complete monolayer coverage (mol/g) and b (L/mol) is a constant that relates to the sorption heat. As shown in Table 2, Langmuir model fits the sorption isotherms better than Freundlich model. The q_e value is found to be smaller than q_{max}, suggesting that CD/HNT/iron oxide surfaces are not saturated and U(VI) is immobilized by a monolayer type. The q_{max} and b values at pH 5.5 are higher than those at pH 4.0, implying a stronger binding of U(VI) on CD/HNT/iron oxide. A smaller n value indicates that the nonlinear sorption process is more favorable at pH 5.5 relative to that at pH 4.0.

The maximum sorption capacity (q_{max}) of CD/HNT/iron oxide towards U(VI) at pH 5.5 was calculated to be 4.52×10^{-4} mol/g (Table 2). In order to verify the feasibility of using CD/HNT/iron oxide composite as a sorbent for wastewater disposal, the maximum sorption capacity (i.e., q_{max} obtained from Langmuir model fitting) of CD/HNT/iron oxide composite towards U(VI) was carefully compared with those reported in previous literatures. As can be seen from Table 3, the sorption capacity of CD/HNT/iron oxide is higher than those of hematite [36], activated carbon [7], oxidized MWCNTs [44] and cross-linked chitosan [45], comparable with MWCNT-g-CMC [46], but lower than that of HA-Zr-PILC [47] and NIMCR [48]. The higher sorption capacity of CD/HNT/iron oxide makes it a suitable material for the removal of U(VI) from large volume solutions.

3.8. Simulated U(VI)-bearing wastewater treatment

In order to corroborate our experimental findings to heterogeneous aquatic systems, we tested the sorption performance of

Table 2
The parameters for Langmuir and Freundlich models.

Conditions		Langmuir			Freundlich		
		q_{max} (mol/g)	b (L/mol)	R^2	K_F ($mol^{1-n} \cdot L^n$/g)	n	R^2
pH 4.5	Sorption	3.31×10^{-4}	5.75×10^3	0.995	0.055	0.641	0.982
	Desorption	3.30×10^{-4}	5.76×10^3	0.994	0.056	0.643	0.983
pH 5.5	Sorption	4.52×10^{-4}	1.37×10^4	0.997	0.025	0.494	0.971
	Desorption	5.91×10^{-4}	2.95×10^4	0.993	0.021	0.441	0.989

Table 3
Comparison of U(VI) sorption capacities of CD/HNT/iron oxide with other sorbents.

Materials	Experimental conditions	q_{max} (mol/g)	References
Hematite	pH = 5.5, T = 298 K	2.35×10^{-5}	[36]
Activated carbon	pH = 3.0, T = 293 K	1.03×10^{-4}	[7]
Oxidized MWCNTs	pH = 5.0, T = 298 K	1.40×10^{-4}	[44]
Cross-linked chitosan	pH = 3.0, T = 298 K	2.70×10^{-4}	[45]
CD/HNT/iron oxide	pH = 5.5, T = 298 K	4.52×10^{-4}	Present study
MWCNT-g-CMC	pH = 5.0, T = 298 K	4.70×10^{-4}	[46]
HA-Zr-PILC	pH = 6.0, T = 303 K	4.81×10^{-4}	[47]
NIMCR	pH = 5.0, T = 298 K	5.90×10^{-4}	[48]

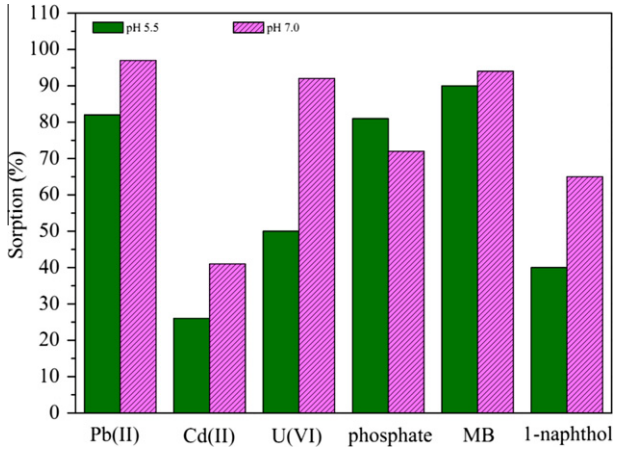

Fig. 10. Removal efficacy of CD/HNT/iron oxide composite towards simulated U(VI)-bearing effluent.

CD/HNT/iron oxide composite towards a simulated wastewater containing various environmental contaminates such as Pb(II) (10 mg/L), Cd(II) (10 mg/L), U(VI) (2.0×10^{-5} mol/L), phosphate (6 mg/L), methylene blue (MB) (50 mg/L) and 1-naphthol (50 mg/L). These components are commonly present in the effluent discharged from textile printing, electroplating, oil refining, fertilizer processing, nuclear power production, etc. Typical experiment was carried out by adding 500 mL mixed wastewater into a 1 L beaker containing 0.5 g/L CD/HNT/iron oxide. The following procedures were conducted as that in batch experiments at two pH values, i.e., pH 5.5 for simulating acid wastewater and pH 7.0 for natural water system. As can be seen from Fig. 10, the removal percentages of CD/HNT/iron oxide towards Pb(II), Cd(II), U(VI), phosphate, MB and 1-naphthol are 82%, 26%, 50%, 81%, 90% and 40% at pH 5.5 and 97%, 41%, 92%, 72%, 94% and 65% at pH 7.0, respectively. The results herein manifests that CD/HNT/iron oxide exhibits satisfying removal efficacy for both inorganic and organic contaminants. Specifically, the efficacy of CD/HNT/iron oxide for the removal of U(VI) from the mixed wastewater is somewhat lower than that from the single-component system. This phenomenon may arise from the combined influence of coexistent heavy metal ions and organic matters in mixed effluent [49]. Further investigations are being considered to verify the application potential of CD/HNT/iron oxide composite as a promising material for actual effluent disposal.

4. Conclusions

In this study, a novel magnetic composite was synthesized by chemically grafting β-CD on HNT/iron oxides particles. The characterization results suggest β-CD has been successfully grafted on HNT/iron oxide surfaces with an amount of 112 mg/g. The obtained CD/HNT/iron oxide composite was used for the removal of U(VI) from aqueous solutions. The sorption performances were investigated by batch technique under various environmental conditions. The accordance of sorption kinetic data with the pseudo-second-order model suggests that chemisorption is the rate-controlling mechanism. The pH-dependent sorption suggests an optimal pH value of 7.0 for using CD/HNT/iron oxide in the decontamination of U(VI) from aqueous solutions. The sorption percentage of U(VI) on CD/HNT/iron oxide was higher than that on bare HNTs and HNT/iron oxides. This enhancement arises from the multiple hydroxyl sites of surface-grafted β-CD. The distinct effects of inorganic/organic ligands on U(VI) immobilization arise from the differences of their affinities to CD/HNT/iron oxide surface sites and their complexation abilities with U(VI). Related data show that the maximum sorption capacity of CD/HNT/iron oxide towards U(VI) is higher than the majority of reported sorbents. Considering the wide raw material sources, simple synthesis procedure, low synthesizing cost, high removal efficiency, environmental friendliness and easy separation of CD/HNT/iron oxide composite, one can make a conclusion that this material may be widely used for the cost-effective treatment of U(VI)-bearing wastewaters. Besides, one can also consider using CD/HNT/iron oxide as a candidate backfilling material for the deep geological disposal of high-level radioactive waste.

Acknowledgements

Financial supports from National Natural Science Foundation of China (41203086; 21107115; 21077107) and National Basic Research Program of China (2011CB933700) are acknowledged.

Appendix A. Supplementary data

Supplementary data associated with this article can be found, in the online version, at http://dx.doi.org/10.1016/j.cej.2012.10.030.

References

[1] A.B. Kersting, D.W. Efurd, D.L. Finnegan, D.J. Rokop, D.K. Smith, J.L. Thompson, Migration of plutonium in ground water at the Nevada test site, Nature 397 (1999) 56–59.
[2] S. Korichi, A. Bensmaili, Sorption of uranium (VI) on homoionic sodium smectite experimental study and surface complexation modeling, J. Hazard. Mater. 169 (2009) 780–793.

[3] R. Schön, G. Winkler, W. Kutschera, A critical review of experimental data for the half-lives of the uranium isotopes ^{238}U and ^{235}U, Appl. Radiat. Isot. 60 (2004) 263–273.
[4] P. Kurttio, A. Auvinen, L. Salonen, H. Saha, J. Pekkanen, I. Mäkeläinen, S.B. Väisänen, I.M. Penttilä, H. Komulainen, Renal effects of uranium in drinking water, Environ. Health Perspect. 110 (2002) 337–342.
[5] K. Skeppström, B. Olofsson, Uranium and radon in groundwater: an overview of the problem, Eur. Water 17 (18) (2007) 51–62.
[6] L.M. Camacho, S. Deng, R.R. Parra, Uranium removal from groundwater by natural clinoptilolite zeolite: effects of pH and initial feed concentration, J. Hazard. Mater. 175 (2010) 393–398.
[7] A. Mellah, S. Chegrouche, M. Barkat, The removal of uranium(VI) from aqueous solutions onto activated carbon: kinetic and thermodynamic investigations, J. Colloid Interface Sci. 296 (2006) 434–441.
[8] H. Parab, S. Joshi, N. Shenoy, R. Verma, A. Lali, M. Sudersanan, Uranium removal from aqueous solution by coir pith: equilibrium and kinetic studies, Bioresour. Technol. 96 (2005) 1241–1248.
[9] K. Akhtar, M.W. Akhtar, A.M. Khalid, Removal and recovery of uranium from aqueous solutions by trichoderma harzianum, Water Res. 41 (2007) 1366–1378.
[10] B.C. Kim, J. Lee, W. Um, J. Kim, J. Joo, J.H. Lee, J.H. Kwak, J.H. Kim, C. Lee, H. Lee, R.S. Addleman, T. Hyeon, M.B. Gu, J. Kim, Magnetic mesoporous materials for removal of environmental wastes, J. Hazard. Mater. 192 (2011) 1140–1147.
[11] X.F. Zhang, C.S. Jiao, J. Wang, Q. Liu, R.M. Li, P.M. Yang, M.L. Zhang, Removal of uranium(VI) from aqueous solutions by magnetic Schiff base: kinetic and thermodynamic investigation, Chem. Eng. J. 198 (199) (2012) 412–419.
[12] R. Fuhrer, I.K. Herrmann, E.K. Athanassiou, R.N. Grass, W.J. Stark, Immobilized β-cyclodextrin on surface-modified carbon-coated cobalt nanomagnets: reversible organic contaminant adsorption and enrichment from water, Langmuir 27 (2011) 1924–1929.
[13] L. Yan, P.R. Chang, P.Y. Zheng, X.F. Ma, Characterization of magnetic guar gum-grafted carbon nanotubes and the adsorption of the dyes, Carbohydr. Polym. 87 (2012) 1919–1924.
[14] N.G. Veerabadran, D. Mongayt, V. Torchilin, R.R. Price, Y.M. Lvov, Organized shells on clay nanotubes for controlled release of macromolecules, Macromol. Rapid Commun. 30 (2009) 99–103.
[15] V. Vergaro, E. Abdullayev, Y.M. Lvov, A. Zeitoun, R. Cingolani, R. Rinaldi, S. Leporatti, Cytocompatibility and uptake of halloysite clay nanotubes, Biomacromolecules 11 (2010) 820–826.
[16] L.X. Song, H.M. Wang, X.Q. Guo, L. Bai, A comparative study on the binding behaviors of β-cyclodextrin and its two derivatives to four fanlike organic guests, J. Org. Chem. 73 (2008) 8305–8316.
[17] P. Yuan, P.D. Southon, Z.W. Liu, M.E.R. Green, J.M. Hook, S.J. Antill, C.J. Kepert, Functionalization of halloysite clay nanotubes by grafting with γ-Aminopropyltriethoxysilane, J. Phys. Chem., C 112 (2008) 15742–15751.
[18] S. Hsieh, B.Y. Huang, S.L. Hsieh, C.C. Wu, C.H. Wu, P.Y. Lin, Y.S. Huang, C.W. Chang, Green fabrication of agar-conjugated Fe_3O_4 magnetic nanoparticles, Nanotechnology 21 (2010) 445601–445606.
[19] R. Chalasani, S. Vasudevan, Cyclodextrin functionalized magnetic iron oxide nanocrystals: a host-carrier for magnetic separation of non-polar molecules and arsenic from aqueous media, J. Mater. Chem. 22 (2012) 14925–14931.
[20] S.S. Banerjee, D.H. Chen, Cyclodextrin conjugated magnetic colloidal nanoparticles as a nanocarrier for targeted anticancer drug delivery, Nanotechnology 19 (2008) 265601–265607.
[21] J.F. Liu, Z.S. Zhao, G.B. Jiang, Coating Fe_3O_4 magnetic nanoparticles with humic acid for high efficient removal of heavy metals in water, Environ. Sci. Technol. 42 (2008) 6949–6954.
[22] Z.G. Wu, W. Feng, Y.Y. Feng, Q. Liu, X.H. Xu, T. Sekino, Preparation and characterization of chitosan-grafted multiwalled carbon nanotubes and their electrochemical properties, Carbon 45 (2007) 1212–1218.
[23] K.G. Bhattacharyya, S.S. Gupta, Influence of acid activation on adsorption of Ni(II) and Cu(II) on montmorillonite: kinetic and thermodynamic study, Chem. Eng. J. 136 (2008) 1–13.
[24] M.S. Chiou, H.Y. Li, Equilibrium and kinetic modeling of adsorption of reactive dye on cross-linked chitosan beads, J. Hazard. Mater. 93 (2002) 233–248.
[25] Y.S. Ho, A.E. Ofomaja, Pseudo-second-order model for lead ion sorption from aqueous solutions onto palm kernel fiber, J. Hazard. Mater. 129 (2006) 137–142.
[26] Y.S. Ho, G. McKay, Comparative sorption kinetic studies of dyes and aromatic compounds onto fly ash, J. Environ. Sci. Health A 34 (1999) 1179–1204.
[27] A. Chen, C. Yang, C. Chen, The chemically crosslinked metal-complexed chitosans for comparative adsorptions of Cu(II), Zn(II), Ni(II), and Pb(II) ions in aqueous medium, J. Hazard. Mater. 163 (2009) 1068–1075.
[28] A. Kowal-Fouchard, R. Drot, E. Simoni, J.J. Ehrhardt, Use of spectroscopic techniques for uranium(VI)/montmorillonite interaction modeling, Environ. Sci. Technol. 38 (2004) 1399–1407.
[29] J.P. Gustafsson, Visual MINTEQ ver. 2.61, Department of land and water resources engineering, KTH Royal Institute of Technology, SE-100 44 Stockholm, Sweden, 2009.
[30] S.T. Yang, G.D. Sheng, X.L. Tan, J. Hu, J.Z. Du, G. Montavon, X.K. Wang, Determination of Ni(II) uptake mechanisms on mordenite surfaces: a combined macroscopic and microscopic approach, Geochim. Cosmochim. Acta 75 (2011) 6520–6534.
[31] S.T. Yang, D.L. Zhao, H. Zhang, S.S. Lu, L. Chen, X.J. Yu, Impact of environmental conditions on the sorption behavior of Pb(II) in Na-bentonite suspensions, J. Hazard. Mater. 183 (2010) 632–640.
[32] A.Z.M. Badruddoza, A.S.H. Tay, P.Y. Tan, K. Hidajat, M.S. Uddin, Carboxymethyl-β-cyclodextrin conjugated magnetic nanoparticles as nano-adsorbents for removal of copper ions: synthesis and adsorption studies, J. Hazard. Mater. 185 (2011) 1177–1186.
[33] C.R. Collins, R.K. Vala, D.M. Sherman, Effect of inorganic and organic ligands on the mechanism of cadmium sorption to goethite, Geochim. Cosmochim. Acta 63 (1999) 2989–3002.
[34] B. Buerge-Weirich, R. Hari, H. Xue, Adsorption of Cu, Cd, and Ni on goethite in the presence of natural groundwater ligands, Environ. Sci. Technol. 36 (2002) 328–336.
[35] M. Villalobos, M.A. Trotz, J.O. Leckie, Surface complexation modeling of carbonate effects on the adsorption of Cr(VI), Pb(II), and U(VI) on goethite, Environ. Sci. Technol. 35 (2001) 3849–3856.
[36] D.L. Zhao, X.B. Wang, S.T. Yang, Z.Q. Guo, G.D. Sheng, Impact of water quality parameters on the sorption of U(VI) onto hematite, J. Environ. Radioact. 103 (2012) 20–29.
[37] U. Hoins, L. Charlet, H. Sticher, Ligand effect on the adsorption of heavy metals: the sulfate–cadmium–goethite case, Water, Air, Soil Pollut. 68 (1993) 241–255.
[38] M.A. Ali, D.A. Dzombak, Competitive sorption of simple organic acids and sulfate on goethite, Environ. Sci. Technol. 30 (1996) 1061–1071.
[39] B.C. Bostick, S. Fendorf, M.O. Barnett, P.M. Jardine, S.C. Brooks, Uranyl surface complexes formed on subsurface media from DOE facilities, Soil Sci. Soc. Am. J. 66 (2002) 99–108.
[40] T. Cheng, M.O. Barnett, E.E. Roden, J.L. Zhuang, Effects of phosphate on uranium(VI) adsorption to goethite-coated sand, Environ. Sci. Technol. 38 (2004) 6059–6065.
[41] C.C. Fuller, J.R. Bargar, J.A. Davis, M.J. Piana, Mechanisms of uranium interactions with hydroxyapatite: implications for groundwater remediation, Environ. Sci. Technol. 36 (2002) 158–165.
[42] M. Shirvani, H. Shaiatmadari, M. Kalbasi, F. Nourbakhsh, B. Najafi, Sorption of cadmium on palygorskite, sepiolite and calcite: equilibria and organic ligand affected kinetics, Colloid Surf., A 287 (2006) 182–190.
[43] M. Businelli, F. Casciari, D. Businelli, G. Gigliotti, Mechanisms of Pb(II) sorption and desorption at some clays and goethite–water interfaces, Agronomie 23 (2003) 219–225.
[44] Y.B. Sun, S.T. Yang, G.D. Sheng, Z.Q. Guo, X.K. Wang, The removal of U(VI) from aqueous solution by oxidized multiwalled carbon nanotubes, J. Environ. Radioact. 105 (2012) 40–47.
[45] G.H. Wang, J.S. Liu, X.G. Wang, Z.Y. Xie, N.S. Deng, Adsorption of uranium(VI) from aqueous solution onto cross-linked chitosan, J. Hazard. Mater. 168 (2009) 1053–1058.
[46] D.D. Shao, Z.Q. Jiang, X.K. Wang, J.X. Li, Y.D. Meng, Plasma induced grafting carboxymethyl cellulose on multiwalled carbon nanotubes for the removal of UO_2^{2+} from aqueous solution, J. Phys. Chem. B 113 (2009) 860–864.
[47] T.S. Anirudhan, C.D. Bringle, S. Rijith, Removal of uranium(VI) from aqueous solutions and nuclear industry effluents using humic acid-immobilized zirconium-pillared clay, J. Environ. Radioact. 101 (2010) 267–276.
[48] L.M. Zhou, C. Shang, Z.R. Liu, G.L. Huang, A.A. Adesina, Selective adsorption of uranium(VI) from aqueous solutions using the ion-imprinted magnetic chitosan resins, J. Colloid Interface Sci. 366 (2012) 165–172.
[49] S.K. Pitcher, R.C.T. Slade, N.I. Ward, Heavy metal removal from motorway stormwater using zeolites, Sci. Total Environ. 334 (335) (2004) 161–166.